HIGH ENERGY pp CHARGED PARTICLE MULTIPLICITY PARAMETERS
(#'s 57, 112, 190, 225, 474, 528, 655, 725, 746, 789, 976, 987)

Presented by J. Whitmore
National Accelerator Laboratory*
Batavia, Illinois

In this report I shall summarize conference contributions reporting on the multiplicity parameters from high-energy pp collisions. I shall also report on some of the new results from the analysis of individual topologies and events from the 205 GeV/c bubble-chamber data from NAL.

Figure 1 shows the topological cross sections[1-5] for high-energy pp interactions. The main features to be noted are:

1. The broadening of the multiplicity distributions as the energy increases. This is due to the fast increase of the high multiplicity cross sections and the slow decrease of the low multiplicity cross sections.

2. The inelastic two-prong, four-prong, and six-prong cross sections are all falling at the highest energies.

3. The eight-prong cross section seems to have reached its maximum at 100-200 GeV/c and is falling at 300 GeV/c.

4. All the other topological cross sections are still increasing at 300 GeV/c.

The low multiplicity cross sections[1-5] are shown in more detail, as a function of incident laboratory momentum, in Fig. 2. The slow energy dependence is perhaps indicative of a diffractive component.

In Fig. 3, the topological cross sections at 100 GeV/c, from the U. Michigan-Rochester collaboration,[3] are shown as a function of the number of negative tracks. The solid curve is from a Nova model calculation by Berger[6] using the parameters found at 28.5 GeV/c. Note, however, that two parameters have to be made energy dependent to fit the data at 200 and 300 GeV/c. The dashed curve is a calculation by Thomas[7] using a multiperipheral model with ρ's being produced according to a Poisson distribution modified by energy, charge, and isospin conservation. At low multiplicities, the production is assumed to have a large diffractive component. There is, however, fair agreement with both curves at the high multiplicities.

Figure 4 shows the preliminary results of a difficult ISR experiment to measure charged particle multiplicities. This is a Pisa-Stony Brook experiment[8] at stationary-target laboratory equivalent momenta of 300, 500, and 1500 GeV/c. Their counters cover almost the entire solid angle. This figure shows their raw multiplicity data. A detailed correction for photon conversion, secondary interactions, finite counter resolution, etc., has not yet been carried out. As a rough

*Operated by Universities Research Association Inc. under contract with the United States Atomic Energy Commission.

estimate of the average charge multiplicity they give: $\langle n_{ch} \rangle = 9.4 \pm 1.5$, 10.4 ± 1.5, and 13 ± 2 at 300, 500, and 1500 GeV/c respectively. The values they give for f_2^{ch} seem high, e.g., at 300 GeV/c they find $f_2^{ch} = 16 \pm 3$, while the value found in the 300 GeV/c bubble-chamber experiment[5] at NAL is $f_2^{ch} = 10.3 \pm 1.9$.

In Fig. 5 are shown the average charged particle multiplicities per inelastic pp collision for bubble-chamber data,[1-5,9] Echo Lake data,[10] various estimates at ISR energies,[8,11-14] and a recent estimate from cosmic rays.[15]

Breidenbach et al.[11] estimate the multiplicity from the charged particle angular distributions for $\theta_{cm} = 30° - 90°$ and from the smaller angle data of Ratner et al.[16] and Bertin et al.[17] by extrapolating with a form $e^{-6.5 p_T}$ to obtain an inclusive rapidity distribution $d\sigma/dy$. The integration of this curve yields $\langle n_{ch} \rangle$ after corrections for $K\bar{K}$ and $N\bar{N}$ pairs and for 1.4 protons per inelastic collision. The estimates from photon production[12,14] are obtained by assuming that $\langle n_{ch} \rangle = \langle n_\gamma \rangle + 1.4$. An estimate at 1500 GeV/c by Damgaard and Hansen[13] was obtained by constructing an empirical formula for the inclusive Lorentz invariant cross section. The integral over x and p_T yields $\langle n_{ch} \rangle$ after corrections for $K\bar{K}$ and $N\bar{N}$ pairs and 1.4 protons. Note that the error bars are only shown for the estimates of Breidenbach et al., but comparable errors are quoted for the other ISR estimates.

The curves in this figure are a) a fit to s^α, yielding $\alpha = 0.28$ when only bubble-chamber data are used[18] (the dashed curve), and b) a fit[19] to the form (solid curve):

$$\langle n_{ch} \rangle = \alpha + \beta \left(1 - \frac{0.93}{p^{0.25}}\right) \ln p \quad \text{with } \alpha = 1.7 \text{ and } \beta = 1.45.$$

The form of this expression is based on parametrizing the growth of the invariant π production cross section $d\sigma/dy$ ($y = 0$), essentially the height of the distribution, and the range of the rapidity (y), essentially the width. Similar forms have been obtained by Breidenbach et al.[11] and Ganguli and Malhotra.[14]

The shape of the multiplicity distribution at any energy may be described by the parameter $F_2^- = \langle n_-(n_- - 1) \rangle$, where n_- is the number of negative particles produced in an interaction. Figure 6 shows F_2^- as a function of p_{lab} for all bubble-chamber data.[1-5] The curves show the dependences expected from a fragmentation and from a multiperipheral model. They are similar below 200 GeV/c but are tending to separate at high energies.

An interesting contribution to this conference is shown in Fig. 7. Wróblewski[20] has observed that all available data below 100 GeV/c lies on a straight line when one plots $D = (\langle n_{ch}^2 \rangle - \langle n_{ch} \rangle^2)^{\frac{1}{2}}$ against $\langle n_{ch} \rangle$. The line is a fit to $D = a\langle n_{ch} \rangle + b$, yielding $a = b = 0.59$. It may be seen that such a form accommodates the new 100, 200, and 300 GeV/c data[3-5] extremely well.

Finally, I shall present some of the results we have obtained from the analysis[21-22] of individual topologies and events in an NAL bubble-chamber experiment at 205 GeV/c. Figure 8 shows a comparison between the rapidity distributions at 28.5 GeV/c[23] and 205 GeV/c for the negative particles from four- and six-prong events. It has been assumed that all negative particles are π^-'s. The low energy data show no indication of a plateau in the central region, in contrast to the 205 GeV/c data which show a plateau but no evidence for any dip at $y_{c.m.} = 0$. This is

perhaps surprising because the high multiplicity events are expected to have a narrower plateau than the low multiplicity events. Consequently, it is unlikely that the total inclusive π^- distribution will show any sizeable plateau in the central region.

Figure 9 shows the rapidity plot (in terms of $y' = \ln \tan \theta/2$) in the laboratory system for a random sample of about fifty 4-18 prong events; the tracks were spatially reconstructed by matching tracks in different views according to bubble patterns. We can conclude that the high multiplicity events do indeed have a narrower plateau region than the low multiplicity events.

Figure 10 shows a p_T^2 distribution for the same sample of 4-18 prongs. The break at $p_T^2 = 0.2\ (\mathrm{GeV/c})^2$ is also observed in lower energy data.

Figure 11 shows the ln tan $\theta/2$ plot for typical individual events at 205 GeV/c. No apparent clustering or lack of clustering is observed. Work is presently underway to parametrize the distributions within individual events in terms of the rapidity dispersion.

References

[1] E. L. Berger, private communication, for pp cross sections and multiplicity parameters for the MSU data between 13 and 28.5 GeV/c.

[2] Soviet-French collaboration, #789,

[3] J. W. Chapman et al., #746.

[4] G. R. Charlton et al., #474.

[5] F. T. Dao et al., #725.

[6] E. L. Berger, private communication.

[7] G. H. Thomas, private communication.

[8] G. Bellettini, private communication.

[9] I. V. Boguslavsky et al., Determination of the Average Charged Particle Multiplicity from 35 GeV/c pp Interactions, JINR, Dubna preprint (unpublished).

[10] L. W. Jones et al., Nucl. Phys. B43, 477 (1972).

[11] M. Breidenbach et al., #528.

[12] G. Neuhofer et al., Phys. Letters 38B, 51 (1972).

[13] G. Damgaard and K. H. Hansen, #112.

[14] S. N. Ganguli and P. K. Malhotra, Phys. Letters 39B, 632 (1972).

[15] S. N. Ganguli and P. K. Malhotra, Dependence of Multiplicity on Energy in High Energy pp Collisions, (TIFR-BC-72-5) and Energy Dependence of $\langle n(n-1)\rangle$ and $\langle n\rangle/D$ in High Energy pp Collisions from $13\text{-}10^4$ GeV/c, (TIFR-BC-72-6).

[16] L. G. Ratner et al., Phys. Rev. Letters 27, 68 (1971).

[17] A. Bertin et al., Phys. Letters 38B, 260 (1972).

[18] E. L. Berger, #225.

[19] T. Ferbel, #655.

[20] A. Wróblewski, #57.

[21] G. R. Charlton et al., #987.

[22] G. R. Charlton et al., #976.

[23] J. Hanlon et al., #190.

[24] See the review talk by J. C. Sens, Results of Experiments on Inclusive Reactions at the CERN Intersecting Storage Rings, presented at the Fourth International Conference on High Energy Collisions, Oxford, England, April 5-7, 1972.

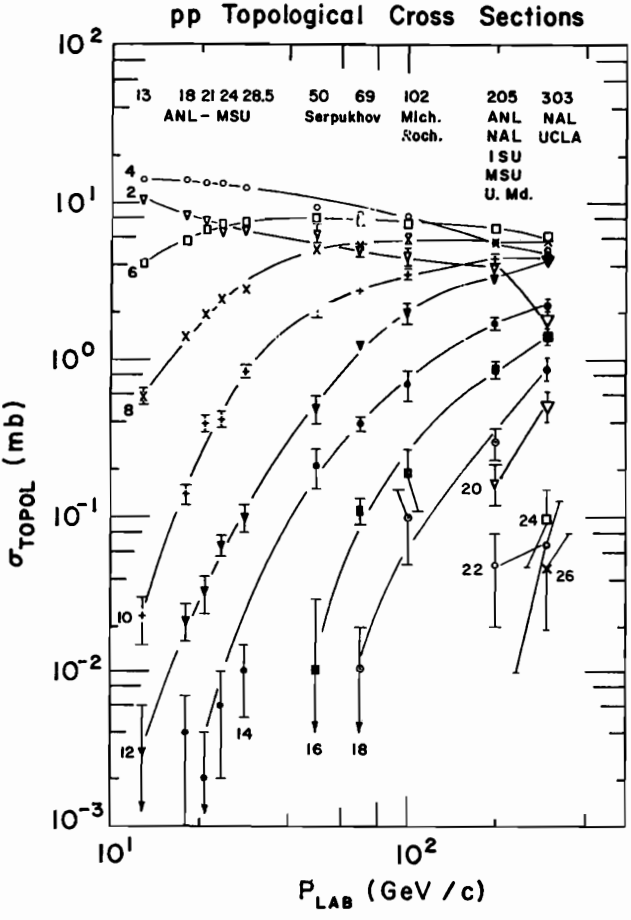

Fig. 1. Topological cross sections for high-energy pp interactions as a function of incident laboratory momentum.

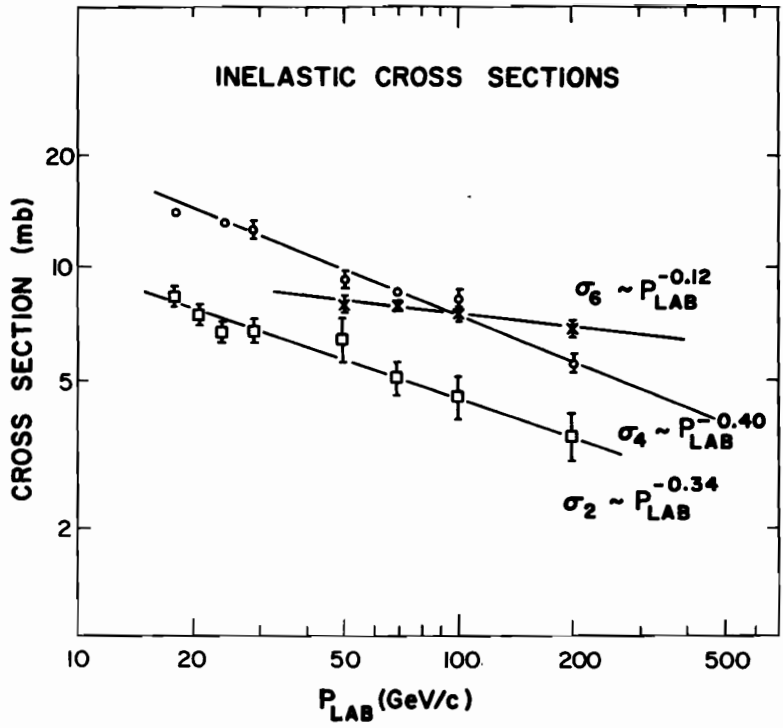

Fig. 2. Low multiplicity inelastic cross sections as a function of incident laboratory momentum.

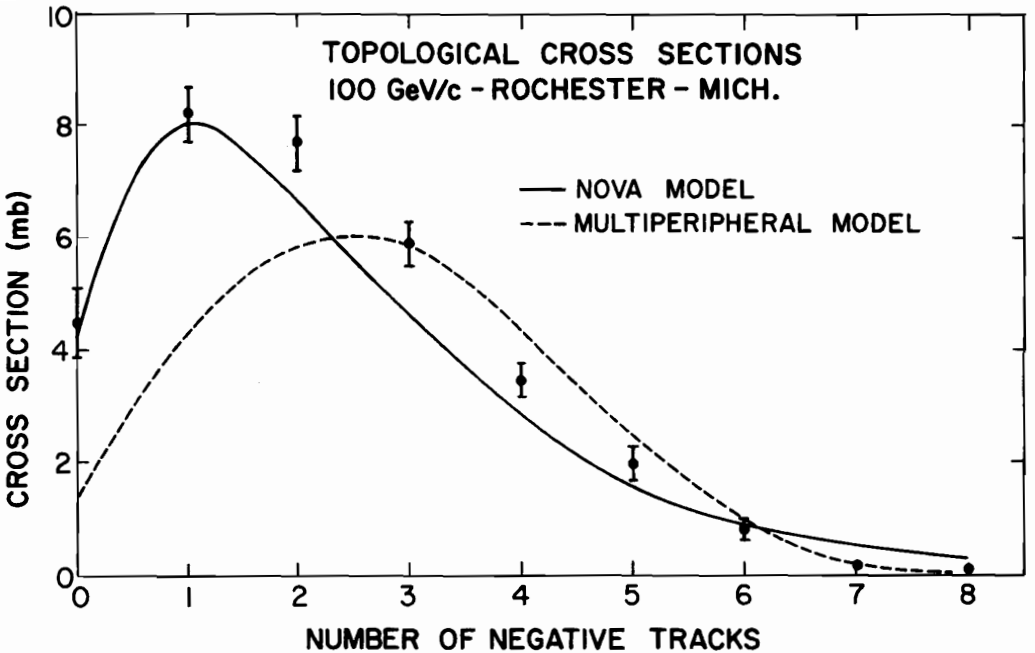

Fig. 3. 100 GeV/c topological cross sections, as a function of the number of negative tracks, compared to the predictions of two models.

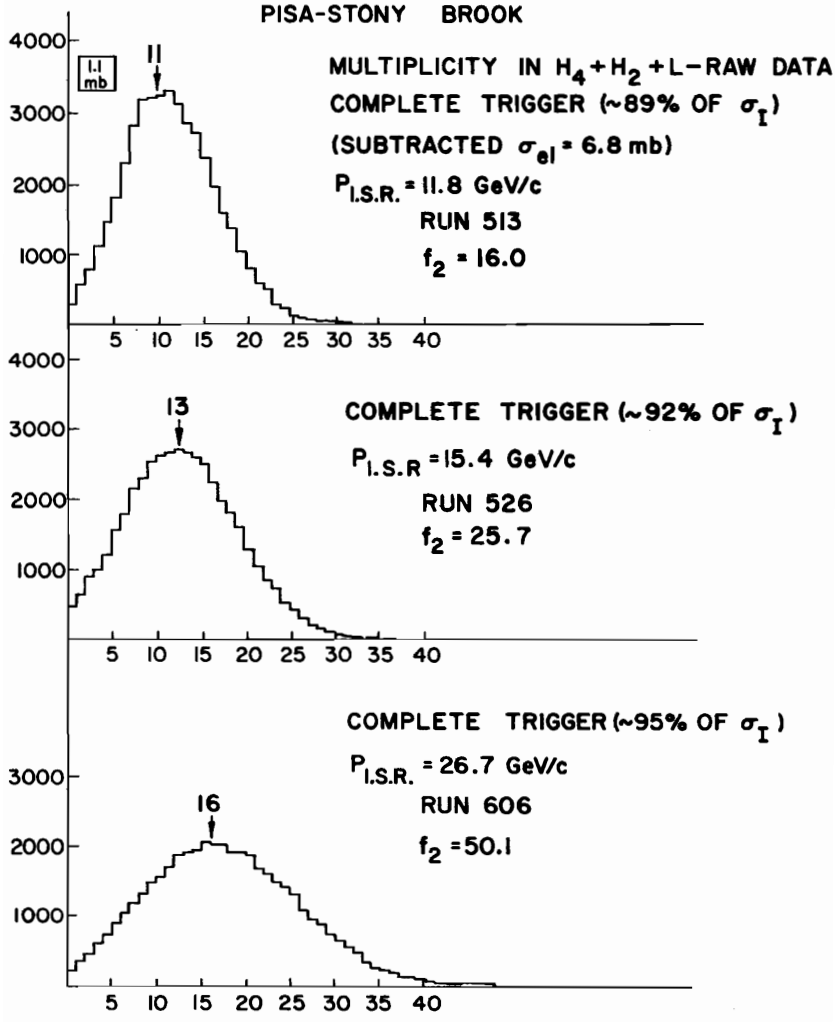

Fig. 4. Preliminary data on charged-particle multiplicities at ISR from Ref. 8.

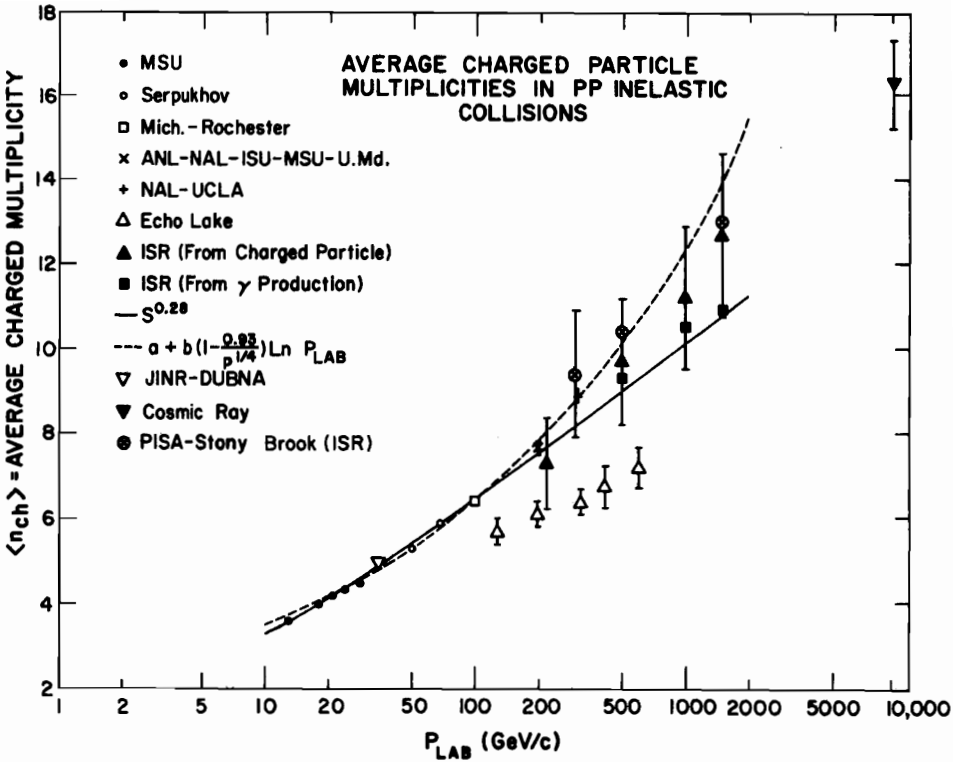

Fig. 5. Average charged-particle multiplicities per inelastic pp collision as a function of incident laboratory momentum.

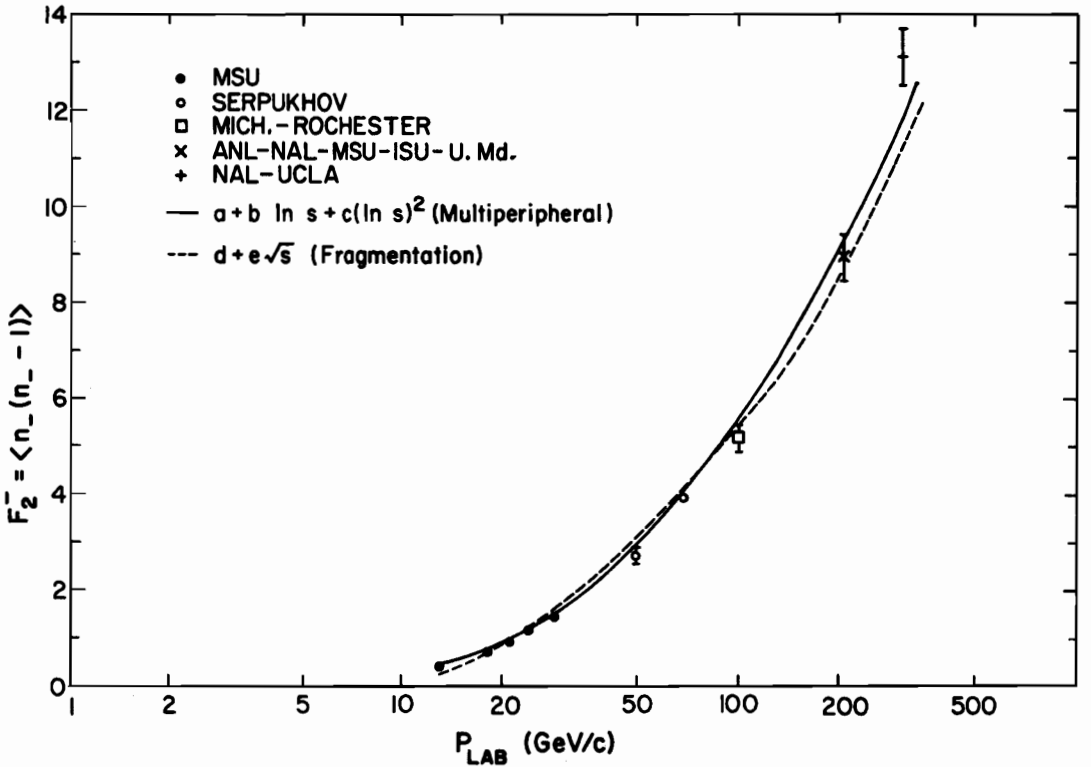

Fig. 6. The F_2^- parameter as a function of p_{lab}.

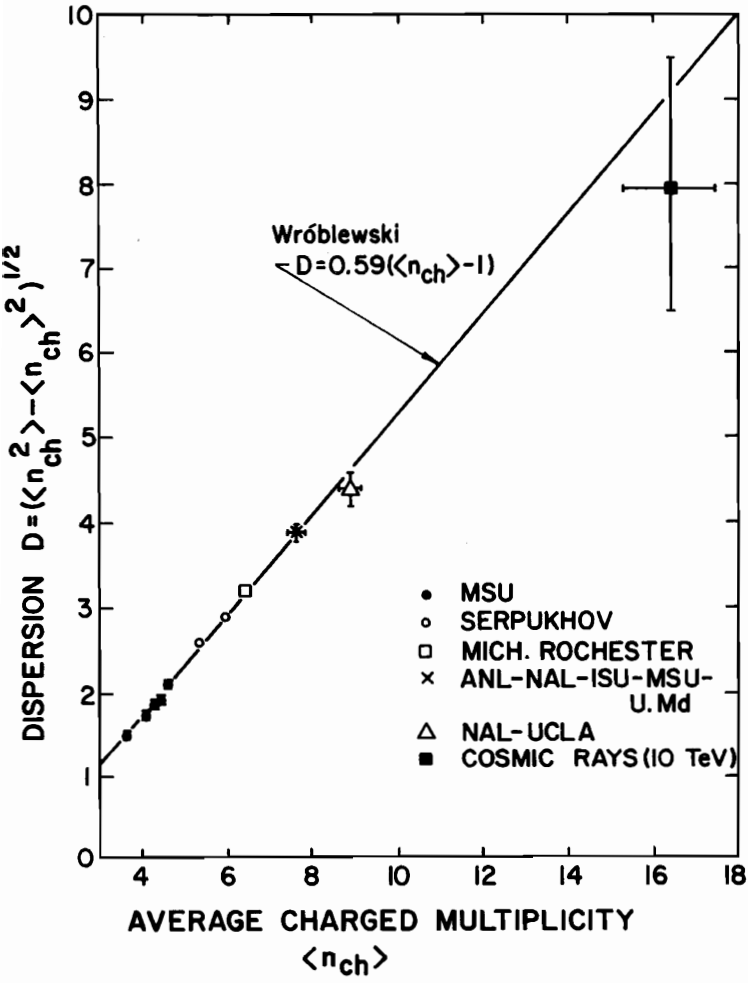

Fig. 7. Plot of the dispersion D as a function of the average charged multiplicity.

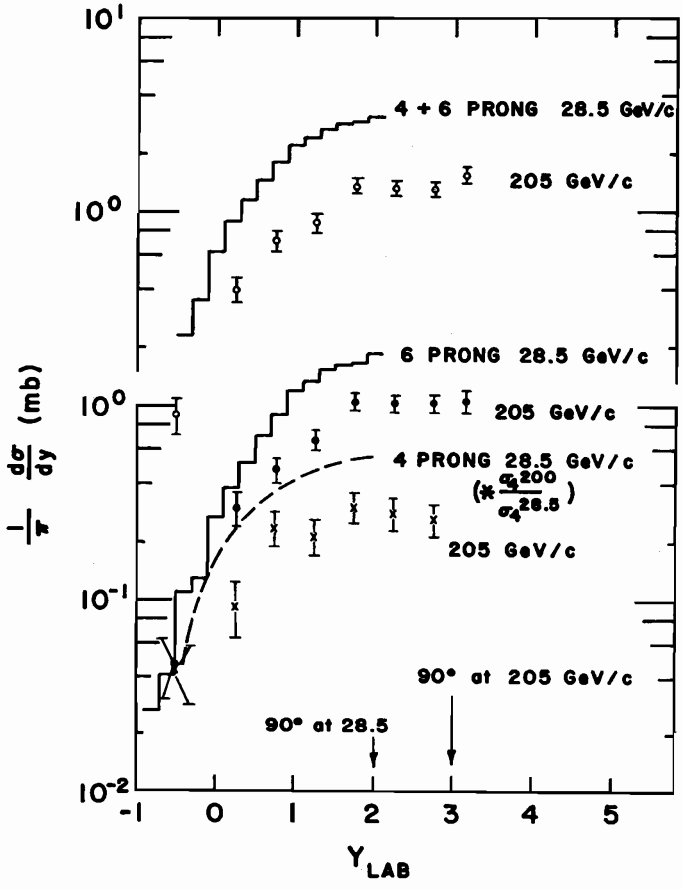

Fig. 8. The differential cross section $\pi^{-1}\, d\sigma/dy$ as a function of the laboratory rapidity y. The solid curves are 28.5 GeV/c data from Ref. 23. The dashed curve is the 28.5 GeV/c data scaled by the relative four-prong topolotical cross sections at 28.5 and 205 GeV/c.

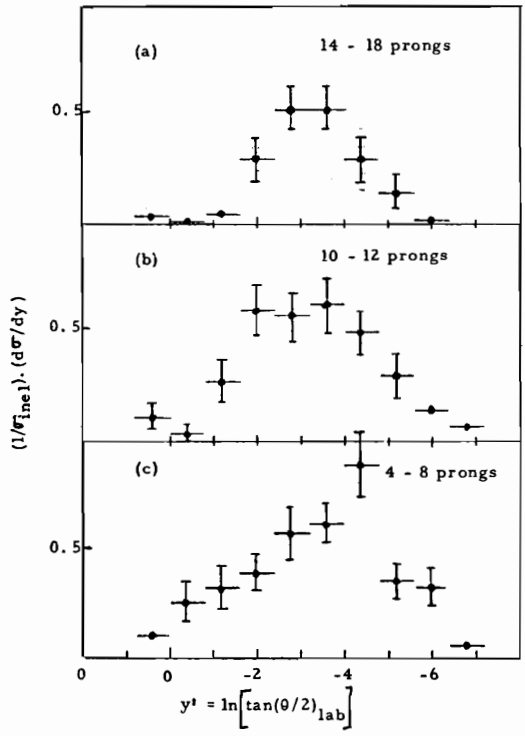

Fig. 9. $\frac{1}{\sigma_{inel}} \frac{d\sigma}{dy'}$ for a) 4-8 prong, b) 10-12 prong, c) 14-18 prong events.

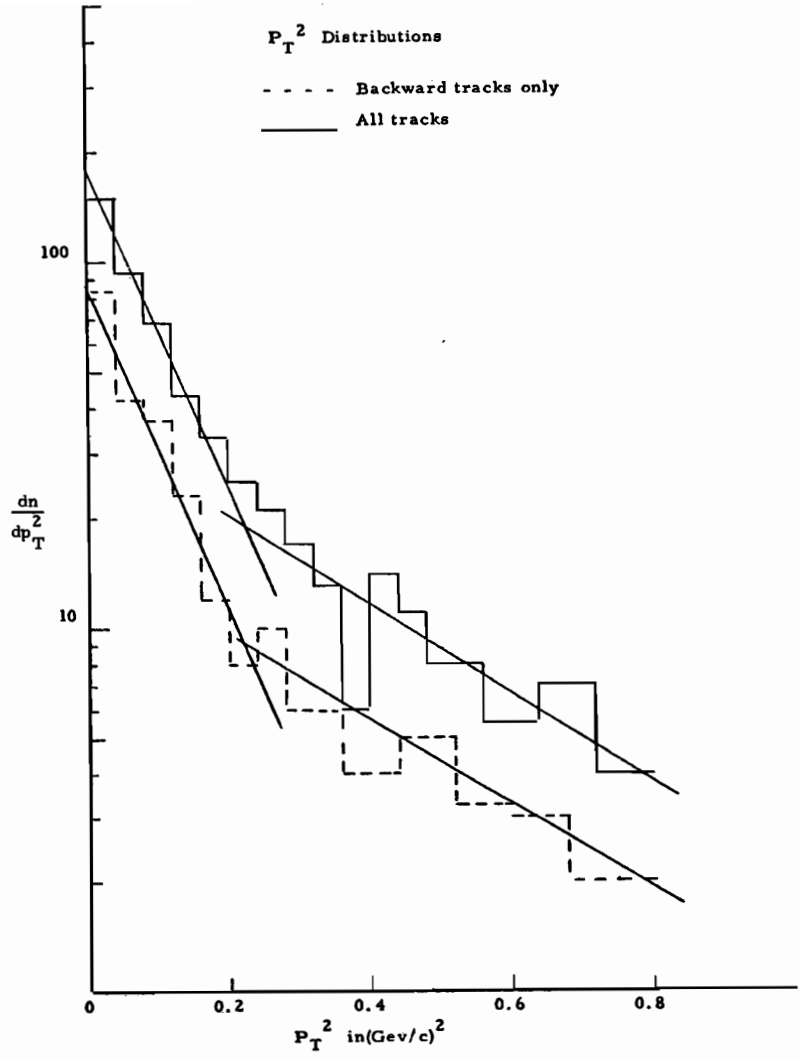

Fig. 10. Transverse momentum squared distribution for a sample of 4-18 prong events at 205 GeV/c. The straight lines are to guide the eye. The steep lines have a slope of $10(\text{GeV/c})^{-2}$; the others have a slope of $4(\text{GeV/c})^{-2}$. The dashed histogram is for those charged particles produced in the backward center-of-mass hemisphere.

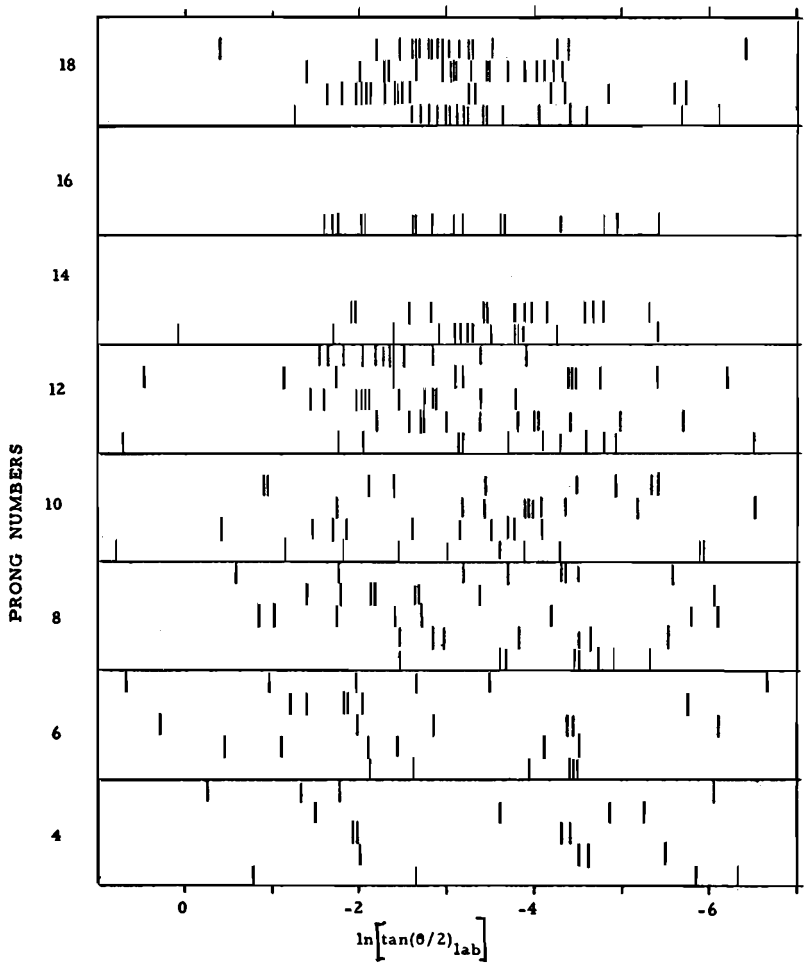

Fig. 11. ln tan $\theta/2$ distribution for individual tracks from a sample of events of various multiplicities at 205 GeV/c.